Self-Interference Cancelation Through Advanced Sampling

Micael Bernhardt, Fernando Gregorio, Juan Cousseau, *Senior Member, IEEE*, and Taneli Riihonen, *Member, IEEE*

***Abstract*—Self-interference is the main obstacle to overcome in order to enable a wireless device to simultaneously transmit and receive in overlapped frequency bands. There is much interest to suppress this interference employing compact and efficient cancelers, which operate in the digital domain, extending this way the benefits of in-band full-duplex to innumerable applications. However, this is not an easy task since the desired signal results hidden in quantization noise during analog-to-digital conversion because of the tremendous power asymmetry between the self-interference and desired signal. This paper proposes an alternative receiver structure in which the received signal is sampled at the zero-amplitude instants of the interference. Our analysis demonstrates that the resulting sampling process preserves the information conveyed in the desired signal and that demodulation is possible. The performance of this novel full-duplex receiver is evaluated using simulations, proving that this sampling strategy enables all digital self-interference cancelation.**

***Index Terms*—Full-duplex, non-uniform sampling, OFDM, self-interference cancellation.**

I. Introduction

SIMULTANEOUS transmission and reception using the same carrier frequencies, known as in-band full-duplex (IBFD), has become a research topic of high interest in recent years. Wireless spectrum is a coveted resource and IBFD promises getting the most out of it, theoretically doubling spectral efficiency and enabling more flexible wireless communication services with higher throughput in a scenario of exponentially growing demand. This new paradigm has the potential to revolutionize spectrum management policies and boost applications like relaying nodes, cell backhauling, small cell- and ad-hoc networks, cognitive radios and carrier aggregation [1]–[3].

One of the main challenges to implement IBFD lies in the fact that the transmitted signal represents an interference with power levels over 100 dB stronger than the desired signal [2]. This is caused by the intrinsic closeness of the interferer with the receiver since they are part of the same communication equipment.

Many previous works have shown that IBFD is achievable using, as a general rule, a chain of interference suppression techniques in various domains [1], [2], [4], [5]. The first step consists of antenna-based (passive) suppression strategies which minimize the electromagnetic self-interference (SI) power captured at the receive port, e.g. physically separating transmit and receive antennas, using different polarizations in their signals, or employing a circulator to isolate them in a single-antenna configuration. With this approach the interference power levels can be reduced around 70 dB [1]. Next, an analog canceler operating at radio frequencies (RF) and/or baseband may subtract a reproduction of the SI from the received signal, potentially achieving further 70 dB of cancellation [1]. At this point, an analog-to-digital converter (ADC) digitalizes the signal and a processor removes any residual interference and compensates for nonlinear distortions occurred in previous phases. Some experiments have shown that the suppression in digital domain can reach several tens of dB [1].

Analog-domain cancelers usually require voluminous, costly and power demanding components which can operate only on limited frequency intervals [2]. Several projects aim to develop integrated analog SI suppressor circuits to enable mass production of smaller and cheaper IBFD capable communication equipment with reduced power consumption [6]. Nevertheless, it is essential for IBFD to develop advanced digital cancelers capable to reduce a greater portion of the interference power [7]. Canceling the strong SI purely in the digital domain is extremely difficult because the dynamic range of the ADCs is absolutely occupied by the SI, and the weak desired signal results concealed in quantization noise [4], [8]. Some research effort has been targeted to improve ADC techniques, increasing the effective resolution after sampling and conversion [9]. *To the best of our knowledge no previous work proposes to*

Manuscript received August 3, 2017; revised November 11, 2017 and December 28, 2017; accepted January 2, 2018. Date of publication January 15, 2018; date of current version February 13, 2018. The associate editor coordinating the review of this manuscript and approving it for publication was Prof. Xin Wang. The work of M. Bernhardt, F. Gregorio, and J. Cousseau was supported in part by the research grant of Agencia Nacional de Promoción Científica y Tecnológica, Argentina, PICT-FONCYT, # 2016-0051: *Aspects of transceiver design for the last generation of wireless communications*, and in part by the research grant of Universidad Nacional del Sur, Argentina, PGI 24/K058: *Signal processing techniques for last generation of wireless transceiver design*. The work of T. Riihonen was supported by the Academy of Finland under Grant 310991. *(Corresponding author: Micael Bernhardt.)*

M. Bernhardt is with the Instituto de Investigaciones en Ingeniería Eléctrica, Universidad Nacional del Sur–Consejo Nacional de Investigaciones Científicas y Técnicas, Bahía Blanca 8000, Argentina, and also with the Departamento de Ingeniería Electrónica, Universidad Nacional de Misiones, Oberá 3360, Argentina (e-mail: mbernhardt@iiie-conicet.gob.ar).

F. Gregorio and J. Cousseau are with the Instituto de Investigaciones en Ingeniería Eléctrica and the Departamento de Ingeniería Eléctrica y de Computadoras, Universidad Nacional del Sur, Bahía Blanca 8000, Argentina (e-mail: fernando.gregorio@uns.edu.ar; jcousseau@uns.edu.ar).

T. Riihonen is with the Laboratory of Electronics and Communications Engineering, Tampere University of Technology, Tampere 33720, Finland (e-mail: taneli.riihonen@tut.fi).

Color versions of one or more of the figures in this paper are available online at http://ieeexplore.ieee.org.

Digital Object Identifier 10.1109/TSP.2018.2793864

sample the received signal at the precise instants when the interference has a zero-amplitude level. This alternative provides interference-free samples of the desired signal and releases the whole ADC dynamic range for its digital conversion. With this method, however, the sampling instants are determined by the known interfering signal and generally differ from the uniformly spaced sample instants used in conventional ADCs.

Non-uniform sampling is natural in fields like radio astronomy, packet data networks and medical applications [10], and there exists abundant bibliography which analyses properties of non-uniformly sampled signals and methods to extract information from them [11]–[15]. Furthermore, some authors have also analyzed unconventional sampling techniques applied to receivers and demodulators [16], [17].

In this work we present following contributions:

- A non-uniform sampling method is introduced, which provides self-interference-free samples of an OFDM transmission without requiring previous cancelers to fit the dynamic range of the signals at the ADC input.
- We show how to generalize the OFDM demodulation process to this new sampling strategy in order to decode the symbols in all subcarriers.
- We present mathematical evidence to prove that this method provides sufficient samples, enabling its application to OFDM transmissions in general.
- The effects of non-ideal sample timing are studied through simulations, showing that the results are valuable and provide high interference suppression levels in non-ideal scenarios.

Section II introduces the system model we used for our analysis, which is generic and easily adaptable to different transceivers for specific applications. Afterwards, Section III explains the special demodulation and decoding techniques developed according to the nonuniform sampling process performed at the receiver. Section IV is devoted to the proof that our interference zero-crossing based sampler is able to preserve enough information about the desired signal to perform its demodulation. The proposed receiver structure is evaluated in Section V using computer-based simulations, where the obtained results support the validity of this new sampling concept. Last, Section VI exposes our conclusions.

II. System Model

This work considers a full-duplex link with two nodes using each a transceiver as shown in Fig. 1. Both remote- and locally transmitted signals employ orthogonal frequency-division modulation (OFDM) techniques with $2N-1$ identical uniformly spaced subcarriers ranging from $f_{-N+1}=(-N+1)/T$ to $f_{N-1}=(N-1)/T$, with T being the OFDM symbol period without the cyclic prefix portion T_{CP}. After the transmit information is processed by the digital modulator and the digital-to-analog converter (DAC), a radio-frequency (RF) mixer translates the signal in frequency domain to center its spectrum around a carrier ω_c tone identical for both transmitters. This produces a perfect overlap of their signal spectra and the transmissions are not orthogonal neither in time nor frequency domains. We also

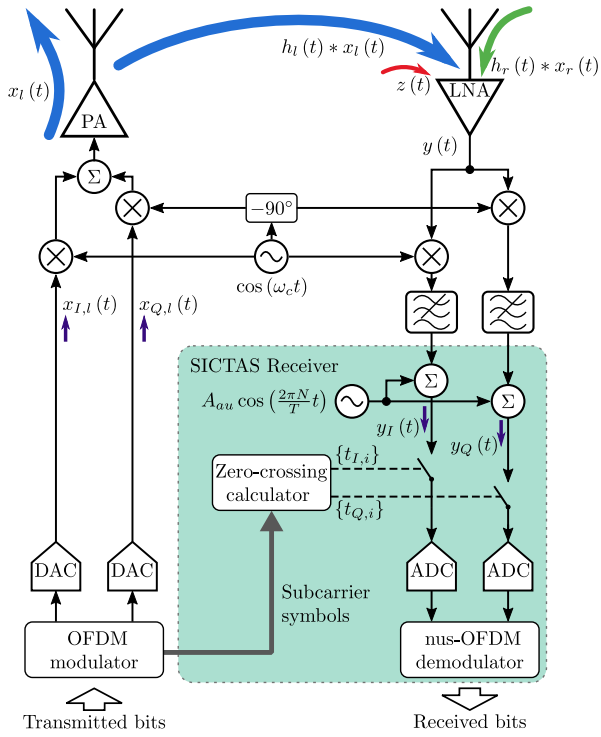

Fig. 1. Block diagram of an in-band full-duplex transceiver. The highlighted block encloses our proposed nonuniform sampling based receiver and demodulator. The RF signals shown are tagged with their baseband equivalent names.

assume that the phase difference Θ_r of the remote carrier with respect to the local one is zero. Finally this passband signal is amplified and emitted through the transmit antenna, using the same power levels at both full-duplex nodes. Since there is no previous SI suppression stage, a significant portion of the local signal power is captured by the receive antenna of the same node, interfering with the desired signal that arrives attenuated by the remote channel.

The received combination of signals is amplified by a low-noise amplifier (LNA) and separated in its real (in-phase) and complex (quadrature) parts mixing it respectively with a cosine and sine waveform tuned at the carrier frequency. After low-pass filtering to eliminate high-frequency aliases, an auxiliary tone is added to both signal branches so that the self-interference zero-crossing rate is maximized. As we will show, the zero-crossing instants are calculated from the transmitted self-interference symbols and are used to drive the sample-and-hold of each branch separately, generating interference-free samples of the remote signal. Last, the ADCs and specific baseband digital processing techniques implemented by a non-uniformly sampled OFDM (nus-OFDM) demodulator obtain the desired information from the samples.

III. Non-Uniformly Sampled OFDM Reception

Conventional OFDM reception is performed by the widely known discrete Fourier transform (DFT) applied to $2N$ uniformly taken samples of the received signal. This operation is concisely expressed by [18]

$$\breve{\mathbf{w}}_r = \mathbf{F}\mathbf{y}, \tag{1}$$

where the application of a normalized DFT matrix $\mathbf{F}$ to vector $\mathbf{y}$ with $2N$ samples of the received complex signal $y(t)$ produces an estimation $\check{\mathbf{w}}_r$ of the symbols modulating $2N$ subcarriers in a desired signal. If the samples in $\mathbf{y}$ are not affected by interference, noise nor channel distortions, the actual transmitted symbols $\mathbf{w}_r$ will be perfectly estimated, i.e. $\check{\mathbf{w}}_r = \mathbf{w}_r$. The element in position (p, q) of the unitary matrix $\mathbf{F}$ is defined by $[\mathbf{F}]_{pq} = (2N)^{-\frac{1}{2}} e^{j\frac{2\pi}{2N}pq}$.

Fig. 1 shows that in a full-duplex scenario the signal $y(t)$ is a superposition of baseband representations for the low-power remotely-transmitted signal of interest $x_r(t)$, the high-power local interference $x_l(t)$ and complex additive white Gaussian noise (AWGN) $z(t)$ with variance σ_z^2. Both modulated signals are affected by the remote and local baseband-equivalent channels $h_r(t)$ and $h_l(t)$ respectively, producing $\tilde{x}_r(t)$ and $\tilde{x}_l(t)$. After these distortions the received signal results

$$\begin{aligned} y(t) &= h_r(t) * x_r(t) + h_l(t) * x_l(t) + z(t) \\ &= \tilde{x}_r(t) + \tilde{x}_l(t) + z(t), \end{aligned} \tag{2}$$

where the symbol $*$ represents a convolution. If the cyclic prefix length of the OFDM symbols is long enough to eliminate inter-block interference (IBI), the convolutions shown above are equivalent to multiplications of the frequency domain representations of the signals and channel impulse responses. By this we can define the channel-distorted symbols vectors for the remote and local OFDM signals as

$$\tilde{\mathbf{w}}_r = \mathbf{H}_r \mathbf{w}_r \tag{3}$$

$$\tilde{\mathbf{w}}_l = \mathbf{H}_l \mathbf{w}_l, \tag{4}$$

where $\mathbf{w}_r$ and $\mathbf{w}_l$ are column vectors containing the remote and local OFDM symbols for all subcarriers, whereas $\mathbf{H}_r$ and $\mathbf{H}_l$ are diagonal matrices with the complex valued gains of the remote and local channels at the corresponding subcarrier positions, respectively. Since we consider two equal IBFD nodes we assume that their signals are transmitted with equal power levels, i.e.

$$\mathbb{E}\left\{\mathbf{w}_r^H \mathbf{w}_r\right\} = \mathbb{E}\left\{\mathbf{w}_l^H \mathbf{w}_l\right\} = \sigma_w^2,$$

where $\mathbb{E}\{\cdot\}$ is the expectation operator.

Equation (1) can be interpreted as a linear transformation which maps the uniform spaced time-domain signal values to an also regular frequency domain grid. We propose a generalization of this linear processing receiver structure, the Self-Interference Cancellation through Advanced Sampling (SICTAS) receiver, relying on separate non-uniform time-domain samples of the in-phase and quadrature components of the received signal to reconstruct the information in the harmonic subcarriers.

Our system produces following estimation for the k-th remote OFDM symbol

$$\check{\mathbf{w}}_r[k] = \mathbf{G}\left(\mathbf{V}_I^{-1}[k]\,\mathbf{y}_I[k] + j\mathbf{V}_Q^{-1}[k]\,\mathbf{y}_Q[k]\right), \tag{5}$$

where $k = 1, 2, \ldots$. Subscript I refers to information processed by the in-phase branch of the receiver, whereas Q represents the quadrature component processing. Within the duration of each symbol k, $2N$ samples are taken separately in each branch according to the non-uniform zero-crossing process of the corresponding self-interference component. Both sample vectors are combined afterwards by the nus-OFDM demodulator using (5), which produces an estimation $\check{\mathbf{w}}_r[k]$ of the actual transmitted symbol vector $\mathbf{w}_r[k]$.

In equation (5) the samples are contained in the column vectors indicated by $\mathbf{y}_I[k]$ and $\mathbf{y}_Q[k]$, and they are drawn respectively from following signals

$$y_I(t) = \Re\{y(t)\} + s_{au}(t) \tag{6}$$

$$y_Q(t) = \Im\{y(t)\} + s_{au}(t). \tag{7}$$

Equation (6) represents the in-phase and (7) the quadrature components of the received baseband signal $y(t)$, each plus an auxiliary tone $s_{au}(t)$ used to maximize the interference zero-crossings.

Matrices $\mathbf{V}_I[k]$ and $\mathbf{V}_Q[k]$ have square Vandermonde structure, and are completely defined by the sampling instant sets $\left\{t_{I,i}^{[k]}\right\}$ and $\left\{t_{Q,i}^{[k]}\right\}$ for the k-th OFDM symbol as follows

$$\mathbf{V}_I[k] = \begin{bmatrix} e^{-j\frac{2\pi}{T}t_{I,1}^{[k]}(N-1)} & \cdots & e^{j\frac{2\pi}{T}t_{I,1}^{[k]}N} \\ \vdots & \ddots & \vdots \\ e^{-j\frac{2\pi}{T}t_{I,2N}^{[k]}(N-1)} & \cdots & e^{j\frac{2\pi}{T}t_{I,2N}^{[k]}N} \end{bmatrix} \tag{8}$$

$$\mathbf{V}_Q[k] = \begin{bmatrix} e^{-j\frac{2\pi}{T}t_{Q,1}^{[k]}(N-1)} & \cdots & e^{j\frac{2\pi}{T}t_{Q,1}^{[k]}N} \\ \vdots & \ddots & \vdots \\ e^{-j\frac{2\pi}{T}t_{Q,2N}^{[k]}(N-1)} & \cdots & e^{j\frac{2\pi}{T}t_{Q,2N}^{[k]}N} \end{bmatrix}. \tag{9}$$

If the sampling instants are pairwise different within each set, the corresponding Vandermonde matrices (8) and (9) are invertible. These inverses produce in (5) a mapping from time to frequency domain equivalent to the DFT used in receivers with uniformly sampled signals, except that in our case the samples are unevenly distributed in an OFDM symbol period.

Last, $\mathbf{G}$ in (5) is the receiver matrix of size $(2N-1) \times (2N)$ defined as

$$\mathbf{G} = \begin{bmatrix} \mathbf{E}\ \mathbf{0} \end{bmatrix}, \tag{10}$$

where $\mathbf{E} = \operatorname{diag}[E_1\ \ldots\ E_{2N-1}]$ is a diagonal frequency-domain equalization matrix whose element E_n compensates for the distortion induced by the remote channel to the n-th subcarrier [18]. We assume that its impulse response is perfectly known at the receiver side, together with the SI channel.

The demodulation process depends on the knowledge of all sampling instants for both branches, i.e. the zero-crossings for both baseband quadrature components of the k-th self-interference OFDM symbol. These instants are determined by the roots found evaluating one counter-clockwise turn on the unit circle $z = e^{j2\pi\tau}$, $\tau \in [0, 1)$ two polynomials

$$\left\{t_{I,i}^{[k]}\right\} = \left\{t_I = \tau T : \sum_{n=0}^{2N} \tilde{a}_{n,l}^{[k]} z^n = 0\right\} \tag{11}$$

$$\left\{t_{Q,i}^{[k]}\right\} = \left\{t_Q = \tau T : \sum_{n=0}^{2N} \tilde{b}_{n,l}^{[k]} z^n = 0\right\}, \tag{12}$$

with $i = 1, \ldots, 2N$ being the root indexes. The polynomial coefficients $\tilde{a}_{n,l}^{[k]}$ and $\tilde{b}_{n,l}^{[k]}$ are obtained from the channel-distorted self-interference symbols modulating the subcarriers, which are perfectly known by the IBFD node. For each SI symbol k the transmitted information varies, and therefore the polynomial coefficients have to be recalculated in a symbol-by-symbol basis. We will show in Section IV how this calculation is performed.

The normalized time index τ refers to the duration of an OFDM symbol without cyclic prefix, which is equivalent to a period T of the fundamental frequency. Therefore, in terms of the absolute time variable t, the samples for each symbol are taken when $t = (k-1)T + kT_{CP} + t_{\{I,Q\},i}^{[k]}$, with $k = 1, 2, \ldots$ and $i = 1, \ldots, 2N$. Setting subscript I or Q selects the absolute sampling instant for the respective signal component.

The rest of this section shows how (5) restores the desired symbols using the non-uniform samples of the remote signal.

Proof of equation (5): Sampling the in-phase baseband signal (6) is equivalent to evaluate the following expression at the instants $\left\{t_{I,i}^{[k]}\right\}, \quad i = 1, \ldots, 2N$

$$y_I(t) = \Re\{\tilde{x}_r(t) + \tilde{x}_l(t)\} + z_I(t) + s_{au}(t),$$

where we used (2) to separate the sampled signal in its components, and $z_I(t) = z(t)\cos(\omega_c t)$. We can group the $2N$ samples of each component in vectors as follows

$$\mathbf{y}_I[k] = \tilde{\mathbf{x}}_{I,r}[k] + \tilde{\mathbf{x}}_{I,l}[k] + \mathbf{z}_I[k] + \mathbf{s}_{au,I}[k], \tag{13}$$

where

$$\begin{aligned}
\mathbf{y}_I[k] &= \left[\, y_I\left(t_{I,1}^{[k]}\right) \quad \ldots \quad y_I\left(t_{I,2N}^{[k]}\right)\right]^T \\
\tilde{\mathbf{x}}_{I,r}[k] &= \Re\left\{\left[\, \tilde{x}_r\left(t_{I,1}^{[k]}\right) \quad \ldots \quad \tilde{x}_r\left(t_{I,2N}^{[k]}\right)\right]^T\right\} \\
\tilde{\mathbf{x}}_{I,l}[k] &= \Re\left\{\left[\, \tilde{x}_l\left(t_{I,1}^{[k]}\right) \quad \ldots \quad \tilde{x}_l\left(t_{I,2N}^{[k]}\right)\right]^T\right\} \\
\mathbf{z}_I[k] &= \left[\, z_I\left(t_{I,1}^{[k]}\right) \quad \ldots \quad z_I\left(t_{I,2N}^{[k]}\right)\right]^T \\
\mathbf{s}_{au,I}[k] &= \left[\, s_{au}\left(t_{I,1}^{[k]}\right) \quad \ldots \quad s_{au}\left(t_{I,2N}^{[k]}\right)\right]^T.
\end{aligned} \tag{14}$$

The same process can be done for the quadrature branch (7), which sampled at the instants $\left\{t_{Q,i}^{[k]}\right\}$ produces

$$\mathbf{y}_Q[k] = \tilde{\mathbf{x}}_{Q,r}[k] + \tilde{\mathbf{x}}_{Q,l}[k] + \mathbf{z}_Q[k] + \mathbf{s}_{au,Q}[k], \tag{15}$$

with

$$\begin{aligned}
\mathbf{y}_Q[k] &= \left[\, y_Q\left(t_{Q,1}^{[k]}\right) \quad \ldots \quad y_Q\left(t_{Q,2N}^{[k]}\right)\right]^T \\
\tilde{\mathbf{x}}_{Q,r}[k] &= \Im\left\{\left[\, \tilde{x}_r\left(t_{Q,1}^{[k]}\right) \quad \ldots \quad \tilde{x}_r\left(t_{Q,2N}^{[k]}\right)\right]^T\right\} \\
\tilde{\mathbf{x}}_{Q,l}[k] &= \Im\left\{\left[\, \tilde{x}_l\left(t_{Q,1}^{[k]}\right) \quad \ldots \quad \tilde{x}_l\left(t_{Q,2N}^{[k]}\right)\right]^T\right\} \\
\mathbf{z}_Q[k] &= \left[\, z_Q\left(t_{Q,1}^{[k]}\right) \quad \ldots \quad z_Q\left(t_{Q,2N}^{[k]}\right)\right]^T \\
\mathbf{s}_{au,Q}[k] &= \left[\, s_{au}\left(t_{Q,1}^{[k]}\right) \quad \ldots \quad s_{au}\left(t_{Q,2N}^{[k]}\right)\right]^T,
\end{aligned} \tag{16}$$

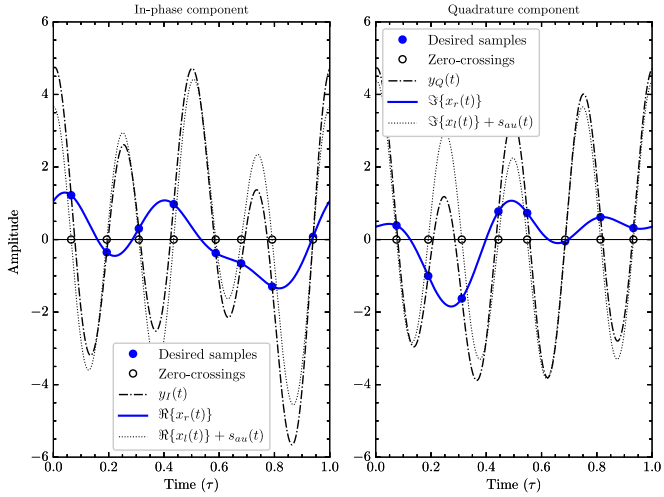

Fig. 2. Details of the signals involved in the sampling process, for the in-phase and quadrature components of a baseband OFDM symbol.

and $z_Q(t) = z(t)\sin(\omega_c t)$. Using the sample vectors (13) and (15) in the receiver equation (5), and omitting the OFDM symbol index $[k]$ for the sake of conciseness, produces

$$\begin{aligned}
\tilde{\mathbf{w}}_r = {} & \mathbf{G}\mathbf{V}_I^{-1}\left[\tilde{\mathbf{x}}_{I,r} + \tilde{\mathbf{x}}_{I,l} + \mathbf{z}_I + \mathbf{s}_{au,I}\right] \\
& + j\mathbf{G}\mathbf{V}_Q^{-1}\left[\tilde{\mathbf{x}}_{Q,r} + \tilde{\mathbf{x}}_{Q,l} + \mathbf{z}_Q + \mathbf{s}_{au,Q}\right].
\end{aligned} \tag{17}$$

To suppress the interference terms in (17) we look for the sampling instants $\{t_{I,i}\}$ and $\{t_{Q,i}\}$ when

$$\begin{aligned}
\Re\{\tilde{x}_l(t_{I,i})\} + s_{au}(t_{I,i}) &= 0 \\
\Im\{\tilde{x}_l(t_{Q,i})\} + s_{au}(t_{Q,i}) &= 0,
\end{aligned}$$

and this should be valid for all instants $i = 1, \ldots, 2N$. This is illustrated in Fig. 2, where the sampling process of the in-phase and quadrature baseband components of a single OFDM symbol with eight subcarriers is exemplified. The highest-, lowest- and zero-frequency components do not carry power, whereas the remaining carriers are modulated with a quadrature-phase shift keying (QPSK) constellation of unit amplitude. The signal generation was done without channel nor noise distortions and using the same powers for the remote and SI signals to highlight the role of all components involved. In both plots it is possible to see that the zero-crossing instants for the SI plus auxiliary tone effectively provide samples of the desired signal without any interference. Note how at these instants the total received signal intersects with the desired remote signal.

Evidently, the signal shapes depend on the information encoded in each transmission, and the sampling process is thus determined by the particular characteristics of the self-interference. Therefore it is important to analyze if the number of zero-crossings in its orthogonal components (i.e. the amount of samples generated by the receiver in each branch) preserves the information carried by the signal of interest. Section IV presents this analysis and finds the requisites to maximize these zero-crossings for real-baseband OFDM signals, since both in-phase and quadrature parts of $\tilde{x}_l(t)$ are real signals themselves.

For the rest of this section we suppose that these conditions are satisfied thanks to the auxiliary tone $s_{au}(t)$, and we continue our analysis using the sampling instant sets obtained with that method. According to this supposition (17) results

$$\begin{aligned}\check{\mathbf{w}}_r &= \mathbf{G}\mathbf{V}_I^{-1}\left[\tilde{\mathbf{x}}_{I,r}+\mathbf{z}_I\right]+j\mathbf{G}\mathbf{V}_Q^{-1}\left[\tilde{\mathbf{x}}_{Q,r}+\mathbf{z}_Q\right]\\ &= \mathbf{G}\left(\mathbf{V}_I^{-1}\tilde{\mathbf{x}}_{I,r}+j\mathbf{V}_Q^{-1}\tilde{\mathbf{x}}_{Q,r}\right)\\ &\quad+\mathbf{G}\left(\mathbf{V}_I^{-1}\mathbf{z}_I+j\mathbf{V}_Q^{-1}\mathbf{z}_Q\right), \end{aligned} \tag{18}$$

where the first term of (18) contains the desired information and the second one is the effective noise $\mathbf{G}\tilde{\mathbf{z}}$ after combining the samples from both branches. Knowing that the received baseband OFDM signal $\tilde{x}_r(t)$ is the sum of $2N-1$ modulated subcarriers, we can write for the i-th element of vector $\tilde{\mathbf{x}}_{I,r}$

$$\begin{aligned}\Re\left\{\tilde{x}_r\left(t_{I,i}\right)\right\} &= \sum_{n=-N+1}^{N-1}\Re\left\{\tilde{w}_{n,r}e^{j\frac{2\pi}{T}nt_{I,i}}\right\}\\ &= \frac{1}{2}\sum_{n=-N+1}^{N-1}\tilde{w}_{n,r}e^{j\frac{2\pi}{T}nt_{I,i}}+\tilde{w}_{n,r}^{*}e^{-j\frac{2\pi}{T}nt_{I,i}}\\ &= \frac{1}{2}\sum_{n=-N+1}^{N-1}\left(\tilde{w}_{n,r}+\tilde{w}_{-n,r}^{*}\right)e^{j\frac{2\pi}{T}nt_{I,i}}, \end{aligned} \tag{19}$$

where $\tilde{w}_{n,r}$ stands for the symbol modulating the n-th subcarrier of the remote signal, weighted by the corresponding channel gain (see (3)).

With the help of an *exchange matrix* $\mathbf{J}$ of size $(2N-1)\times(2N-1)$ defined by

$$\mathbf{J}_{(p,q)}=\begin{cases}1, & q=2N-p\\ 0, & q\neq 2N-p\end{cases},$$

and using (8), expression (19) can be converted into matrix form to calculate all elements of vector $\tilde{\mathbf{x}}_{I,r}$ as follows

$$\tilde{\mathbf{x}}_{I,r}=\frac{1}{2}\mathbf{V}_I\left(\begin{bmatrix}\tilde{\mathbf{w}}_r\\0\end{bmatrix}+\begin{bmatrix}\mathbf{J}\tilde{\mathbf{w}}_r^{*}\\0\end{bmatrix}\right). \tag{20}$$

Vector $\tilde{\mathbf{x}}_{Q,r}$ can be obtained by a similar deduction. Its i-th element results

$$\begin{aligned}\Im\left\{\tilde{x}_r\left(t_{Q,i}\right)\right\} &= \sum_{n=-N+1}^{N-1}\Im\left\{\tilde{w}_{n,r}e^{j\frac{2\pi}{T}nt_{Q,i}}\right\}\\ &= \frac{j}{2}\sum_{n=-N+1}^{N-1}\tilde{w}_{-n,r}^{*}e^{j\frac{2\pi}{T}nt_{Q,i}}-\tilde{w}_{n,r}e^{-j\frac{2\pi}{T}nt_{Q,i}}\\ &= \frac{j}{2}\sum_{n=-N+1}^{N-1}\left(\tilde{w}_{-n,r}^{*}-\tilde{w}_{n,r}\right)e^{j\frac{2\pi}{T}nt_{Q,i}}, \end{aligned} \tag{21}$$

whereas the expression for vector $\tilde{\mathbf{x}}_{Q,r}$ is found from (21) with the help of (9)

$$\tilde{\mathbf{x}}_{Q,r}=\frac{j}{2}\mathbf{V}_Q\left(\begin{bmatrix}\mathbf{J}\tilde{\mathbf{w}}_r^{*}\\0\end{bmatrix}-\begin{bmatrix}\tilde{\mathbf{w}}_r\\0\end{bmatrix}\right). \tag{22}$$

Using (20) and (22) in (18) produces

$$\begin{aligned}\check{\mathbf{w}}_r &= \frac{1}{2}\mathbf{G}\left[\mathbf{V}_I^{-1}\mathbf{V}_I\left(\begin{bmatrix}\tilde{\mathbf{w}}_r\\0\end{bmatrix}+\begin{bmatrix}\mathbf{J}\tilde{\mathbf{w}}_r^{*}\\0\end{bmatrix}\right)\right.\\ &\quad\left.-\ \mathbf{V}_Q^{-1}\mathbf{V}_Q\left(\begin{bmatrix}\mathbf{J}\tilde{\mathbf{w}}_r^{*}\\0\end{bmatrix}-\begin{bmatrix}\tilde{\mathbf{w}}_r\\0\end{bmatrix}\right)\right]+\mathbf{G}\tilde{\mathbf{z}}\\ &= \mathbf{G}\begin{bmatrix}\tilde{\mathbf{w}}_r\\0\end{bmatrix}+\mathbf{G}\tilde{\mathbf{z}}\\ &= \mathbf{E}\tilde{\mathbf{w}}_r+\mathbf{G}\tilde{\mathbf{z}}\\ &= \mathbf{E}\mathbf{H}_r\mathbf{w}_r+\mathbf{G}\tilde{\mathbf{z}}, \end{aligned} \tag{23}$$

where in the last line we used (3).

Equation (23) shows that after channel distortion compensation by means of an equalizer, the estimated symbols are only affected by the effective noise term $\mathbf{G}\tilde{\mathbf{z}}$. Through this sampling process all interference is eliminated and the bottleneck for digital SI cancellation is avoided.

The demodulation process requires calculating the inverse of a Vandermonde matrix for each OFDM symbol. Nevertheless, there exist methods to compute in explicit form the components of these inverse matrices [19]–[21]. Even more, if the transceiver has a transmit buffer it can pre-calculate the SI zero-crossings and inverse Vandermonde matrices before actually sending these signals, minimizing the potential latency caused by their computation in real time.

IV. Zero-Crossing Determination for Real Baseband OFDM Signals

OFDM systems encode information in a signal obtained from the sum of harmonic subcarriers, each weighted by a complex symbol which represents a predefined combination of bits, modifying this way in a specific manner the subcarriers amplitudes and/or phases. This sum of harmonic tones defines an OFDM symbol with a period reciprocal of the smallest subcarrier frequency. Though these symbols are afterwards concatenated to transmit a greater amount of information, we analyze the zero-crossings for an isolated OFDM symbol and thus consider it a signal with period T.

Furthermore, since complex-baseband symbols can be represented as two associated real-valued signal streams which can be processed separately, the analysis presented can be circumscribed to zero-crossings of periodic real-valued interference signals.

Let $s(t)$ be a continuous-time and baseband real signal with period of T seconds and following Fourier series representation

$$s(t)=\sum_{n=-N}^{N}c_n e^{j\frac{2\pi}{T}nt}. \tag{24}$$

This signal has a double-sided bandwidth of size $2W=2N/T$, which is $2N$ times the fundamental frequency. Since $s(t)$ is real, the complex coefficients c_n satisfy following condition

$$c_{-n}=c_n^{*},\qquad n=0,1,2,\ldots,N, \tag{25}$$

which also implies that $c_0=c_0^{*}$ has to be real.

We can introduce following variable substitution

$$z = e^{j\frac{2\pi}{T}t}, \tag{26}$$

and this way the series in (24) is transformed into

$$\begin{aligned} S(z) &= \sum_{n=-N}^{N} c_n z^n \\ &= z^{-N} \sum_{n=0}^{2N} c_{n-N} z^n \\ &= z^{-N} P(z), \end{aligned} \tag{27}$$

which can be interpreted as a transfer function whose first factor is a pole with multiplicity N on $z = 0$, and the factor $P(z)$ is a polynomial of order $2N$ in the complex plane. By the fundamental theorem of algebra we know that this polynomial provides exactly $2N$ zeros to (27).

We are interested in finding the instants when signal $s(t)$ equals to zero, and due to substitution (26) we can see that a cycle of the signal $s(t)$ corresponds to evaluate expression (27) one counter-clockwise turn on the unit circle. Thus, the problem of finding the zero crossings of $s(t)$ during one period T is equivalent to finding the different roots of polynomial $P(z)$ located on the unit circle. It easily follows that the maximum possible number of zero-crossings is equal to the order of $P(z)$. If this polynomial has roots with non-unitary magnitude, the corresponding real signal has *complex zeros* [22].

By (25) we can see that the polynomial $P(z)$ in (27) is self-inversive. Corollary 3 of [23] states that all roots of a self-inversive polynomial are simple and located on the unit circle if and only if any of three conditions presented in the reference is satisfied by its coefficients. Applied to $P(z)$ these conditions are

$$|c_N| > \frac{1}{2} \sum_{n=-N}^{N-1} |c_{n+1} - c_n| \tag{28}$$

$$|c_N| > \sum_{n=-N+1}^{N-1} |c_N - c_n| \tag{29}$$

$$|c_N| > \frac{1}{2} \sum_{n=-N+1}^{N-1} |c_n|. \tag{30}$$

These expressions define the spectral energy distribution for a real signal to achieve the maximum of $2N$ zero crossings in a period T. In our system this is equivalent to a mean rate of $2N/T$ samples per second enabling us to receive a signal whose highest frequency component is $f_{max} = 1/2 \times 2N/T = N/T$, which is slightly higher than the maximum spectral component of the desired signal.

Inequalities (28) through (30) have to be tested for different modulation techniques in order to assure that the number of zero-crossings during one period T is enough to sample a similarly modulated signal without loss of information. If any of these conditions is satisfied the system will be able to produce self-interference-free samples and perform IBFD transmissions. Otherwise, the signal $s(t)$ may be suitably modified with that aim.

This same method has been applied in [24], where an auxiliary tone of appropriate frequency and amplitude is summed to an input signal before deriving it to a zero-crossing detector with the purpose to perform a spectral analysis. In a similar manner, for our system it is possible to add a tone of sufficient amplitude with frequency $f_{au} = N/T$ Hz to the interference and modify its spectral composition to comply with any of (28) to (30). This modification should preferably be done at the receive stage, since otherwise the tone represents an important increment in the transmitted power. After that addition, the resulting signal will have $2N$ zero-crossings distributed close to the zeros of the auxiliary signal, with deviations given by the particular OFDM symbol transmitted during the analyzed period.

The Fourier series expansions for the real and imaginary parts of a baseband OFDM self-interference symbol $\tilde{x}_l(t)$ can be expressed as in (19) and (21), resulting

$$\begin{aligned} \Re\{\tilde{x}_l(t)\} &= \sum_{n=-N+1}^{N-1} \Re\left\{\tilde{w}_{n,l} e^{j\frac{2\pi}{T}nt}\right\} \\ &= \frac{1}{2} \sum_{n=-N+1}^{N-1} \tilde{w}_{n,l} e^{j\frac{2\pi}{T}nt} + \tilde{w}^*_{n,l} e^{-j\frac{2\pi}{T}nt} \\ &= \frac{1}{2} \sum_{n=-N+1}^{N-1} \left(\tilde{w}_{n,l} + \tilde{w}^*_{-n,l}\right) e^{j\frac{2\pi}{T}nt} \\ &= \frac{1}{2} \sum_{n=-N+1}^{N-1} a_{n,l} e^{j\frac{2\pi}{T}nt} \end{aligned} \tag{31}$$

$$\begin{aligned} \Im\{\tilde{x}_l(t)\} &= \sum_{n=-N+1}^{N-1} \Im\left\{\tilde{w}_{n,l} e^{j\frac{2\pi}{T}nt}\right\} \\ &= \frac{1}{2} \sum_{n=-N+1}^{N-1} j\tilde{w}^*_{n,l} e^{-j\frac{2\pi}{T}nt} - j\tilde{w}_{n,l} e^{j\frac{2\pi}{T}nt} \\ &= \frac{1}{2} \sum_{n=-N+1}^{N-1} j\left(\tilde{w}^*_{-n,l} - \tilde{w}_{n,l}\right) e^{j\frac{2\pi}{T}nt} \\ &= \frac{1}{2} \sum_{n=-N+1}^{N-1} b_{n,l} e^{j\frac{2\pi}{T}nt}, \end{aligned} \tag{32}$$

where $a_{n,l} = (\tilde{w}_{n,l} + \tilde{w}^*_{-n,l})$ and $b_{n,l} = j(\tilde{w}^*_{-n,l} - \tilde{w}_{n,l})$, and the coefficients $\{\tilde{w}_{n,l}\}$ are the elements of vector (4). It is fairly simple to verify that the sets of coefficients $\{a_{n,l}\}$ and $\{b_{n,l}\}$ generate self-inversive polynomials, but in general none of conditions (28) to (30) is satisfied. The auxiliary sampling signal $s_{au}(t)$ we add to the in-phase and quadrature branches modifies expressions (31) and (32) to assure that for both of them at least one of these conditions is satisfied. Specifically, we design this auxiliary signal to be following cosine function

$$\begin{aligned} s_{au}(t) &= A_{au} \cos(2\pi f_{au} t) \\ &= \frac{A_{au}}{2} \left(e^{j\frac{2\pi}{T}Nt} + e^{-j\frac{2\pi}{T}Nt}\right), \end{aligned} \tag{33}$$

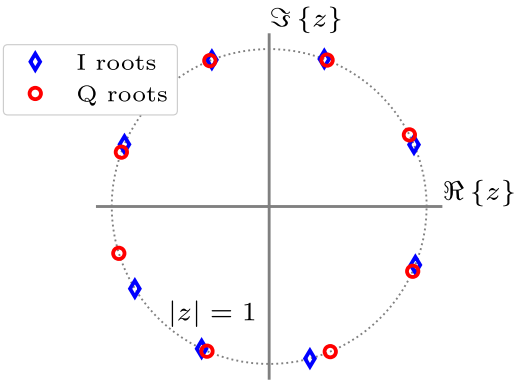

Fig. 3. Root location of the polynomials obtained for the in-phase (I) and quadrature (Q) parts of the self-interference plus auxiliary sampling tones shown in Fig. 2.

with $A_{au} > 0$. Its addition to (31) and (32) introduces two real coefficients in their associated polynomials in z, more precisely at the highest- and zero-exponent terms, preserving their self-reciprocity. Thus we can write

$$\Re\{\tilde{x}_l(t)\} + s_{au}(t) = \frac{1}{2}\sum_{n=-N}^{N} \tilde{a}_{n,l} e^{j\frac{2\pi}{T}nt} \tag{34}$$

$$\Im\{\tilde{x}_l(t)\} + s_{au}(t) = \frac{1}{2}\sum_{n=-N}^{N} \tilde{b}_{n,l} e^{j\frac{2\pi}{T}nt}, \tag{35}$$

where the coefficients $\tilde{a}_{n,l}$ and $\tilde{b}_{n,l}$ are given by

$$\tilde{a}_{n,l} = \begin{cases} A_{au}, & \text{if } n = \pm N \\ a_{n,l}, & \text{if } -N+1 \le n \le N-1 \end{cases} \tag{36}$$

$$\tilde{b}_{n,l} = \begin{cases} A_{au}, & \text{if } n = \pm N \\ b_{n,l}, & \text{if } -N+1 \le n \le N-1 \end{cases}. \tag{37}$$

These are the sets of coefficients to construct polynomials (11) and (12), and they are totally defined by the SI modulating symbols, the loop-back channel response and the auxiliary sampling signal. In Appendix A we show that only condition (30) can be satisfied simultaneously for these new polynomials (see (45)), provided that

$$A_{au} > \sum_{n=-N+1}^{N-1} |\tilde{w}_{n,l}|. \tag{38}$$

This inequality establishes the minimum amplitude of A_{au} in order to guarantee that all zeros of the polynomials with coefficients obtained from (34) and (35) are located on the unit circle. Consequently, the zero-crossing rate for both interference components is maximized and our nonuniform sampling method will produce sufficient samples to preserve the information encoded in the signal of interest.

Fig. 3 illustrates the root locations for the polynomials obtained from the real and imaginary part of the SI signal exemplified in Fig. 2, each summed with the auxiliary sampling cosine with amplitude

$$A_{au} = 1.10 \times A_w N_m,$$

where A_w is the maximum symbol amplitude in the constellation and N_m is the number of subcarriers with nonzero power. Note that, since this example does not implement channel distortions, the selected amplitude A_{au} has an $10\,\%$ margin with respect to the bound in (38). The roots were found using a root finding algorithm, and because all of them lie on the unit circle and have multiplicity equal to one, this produces $2N$ zero-crossings for the corresponding signals verified in Fig. 2. The complexity of finding the polynomial roots depends not only on the approximation method chosen but also on the initial estimations and admissible timing error, and therefore it is difficult to express universally the costs associated to this task. For a literature review on this subject we refer to [25] and references therein.

If we consider the special case of single-carrier digital transceivers, which can be thought of as OFDM systems where all but the highest subcarriers have zero power, it is simple to verify that they satisfy condition (30). This holds as long as this carrier does not vanish nor changes its frequency as it happens in on-off keying or frequency-shift keying transmissions. If the digital modulation technique employed guarantees the presence of a frequency-stable carrier, the zero-crossing rate of the SI is already high enough to preserve the information in the remote signal without requiring an auxiliary tone to be added before sampling. Consequently the receiver structure is simplified, whereas the reception process of Section III remains unchanged for these single-carrier receivers.

This property can be used to obtain uniform samples and estimate the remote channel $h_r(t)$. The local transmitter is deactivated during this phase to produce an interference-free estimation, and the zero-crossings will be only determined by the auxiliary sampling tone $s_{au}(t)$. Therefore, the samples obtained will have an uniform distribution and the frequency domain response of the remote channel as well as its equalizer may be calculated using conventional methods.

In the next Subsection we will analyze the stochastic behavior of the zero-crossing process for OFDM signals, which gives us an important result to derive the average symbol estimation error power induced by our receive process in Subsection IV-B.

A. *Expected Zero-Crossing Process for Real Baseband OFDM*

If we consider that the constellations used to encode the transmitted groups of bits in the OFDM subcarriers are designed so they have zero mean value, then

$$\mathbb{E}\{w_{n,l}\} = 0,\ n = -N+1, \ldots, N-1. \tag{39}$$

Furthermore, assuming independence among all subcarriers we can find that the expected polynomial coefficients in (36) and (37) are

$$\mathbb{E}\{\tilde{a}_{n,l}\} = \begin{cases} A_{au}, & \text{if } n = \pm N \\ \mathbb{E}\{a_{n,l}\} = 0, & \text{if } -N+1 \le n \le N-1 \end{cases}$$

$$\mathbb{E}\left\{\tilde{b}_{n,l}\right\} = \begin{cases} A_{au}, & \text{if } n = \pm N \\ \mathbb{E}\{b_{n,l}\} = 0, & \text{if } -N+1 \le n \le N-1 \end{cases}.$$

This means that the expected polynomials for the in-phase and quadrature signals are both equal to

$$\bar{P}(z) = A_{au}\left(1 + z^{2N}\right),$$

whose roots are given by

$$z^{2N} = -1 = e^{j\pi}$$
$$z = e^{j\left(\frac{\pi}{2N} + r\frac{\pi}{N}\right)},\ r = 0, 1, \ldots, 2N-1.$$

This result tells us that the polynomial zeros coincide with the $2N$ roots of unity rotated by $\pi/2N$ radians, and therefore selecting a cosine as our auxiliary signal for both branches ensures us that the expected sampling process is uniformly distributed in time, namely at the instants

$$t_{I,i} = t_{Q,i} = t_i = \frac{T}{2N}\left(i - \frac{1}{2}\right), \quad i = 1, 2, \ldots, 2N,$$

and therefore the expected Vandermonde matrices (8) and (9) also result equal

$$\mathbb{E}\{\mathbf{V}_I\} = \mathbb{E}\{\mathbf{V}_Q\}$$
$$= \begin{bmatrix} e^{-j\frac{\pi}{N}\left(\frac{1}{2}\right)(N-1)} & \cdots & e^{j\frac{\pi}{N}\left(\frac{1}{2}\right)N} \\ \vdots & \ddots & \vdots \\ e^{-j\frac{\pi}{N}\left(\frac{4N-1}{2}\right)(N-1)} & \cdots & e^{j\frac{\pi}{N}\left(\frac{4N-1}{2}\right)N} \end{bmatrix}.$$

It can also be shown that

$$\mathbb{E}\left\{\mathbf{V}_I^H\mathbf{V}_I\right\} = \mathbb{E}\left\{\mathbf{V}_Q^H\mathbf{V}_Q\right\} = 2N\mathbf{I}, \tag{40}$$

which means that, up to a scaling, the expected Vandermonde matrices are unitary. This result is very useful for next subsection.

B. Average Symbol Estimation Error Power

The estimation error is defined as the difference between the estimated vector of symbols in (23) and the ideal ones

$$\mathbf{e}_w = \check{\mathbf{w}}_r - \mathbf{w}_r$$
$$= \mathbf{G}\left(\mathbf{V}_I^{-1}\mathbf{z}_I + j\mathbf{V}_Q^{-1}\mathbf{z}_Q\right).$$

TABLE I
OFDM PARAMETERS USED IN THE SIMULATIONS

Number of subcarriers	Guard band size	Constellation
512	212	16-QAM
1024	424	16-QAM
2048	848	16-QAM

This way we can calculate the estimation error power as

$$\sigma_e^2 = \mathbb{E}\left\{\mathbf{e}_w^H\mathbf{e}_w\right\}$$
$$= \mathbb{E}\left\{\left(\mathbf{z}_I^H\mathbf{V}_I^{-H} - j\mathbf{z}_Q^H\mathbf{V}_Q^{-H}\right)\mathbf{G}^H\mathbf{G}\mathbf{V}_I^{-1}\mathbf{z}_I\right\}$$
$$+ j\mathbb{E}\left\{\left(\mathbf{z}_I^H\mathbf{V}_I^{-H} - j\mathbf{z}_Q^H\mathbf{V}_Q^{-H}\right)\mathbf{G}^H\mathbf{G}\mathbf{V}_Q^{-1}\mathbf{z}_Q\right\}$$
$$= \mathbb{E}\left\{\mathbf{z}_I^H\mathbf{V}_I^{-H}\mathbf{G}^H\mathbf{G}\mathbf{V}_I^{-1}\mathbf{z}_I\right\}$$
$$- j\mathbb{E}\left\{\mathbf{z}_Q^H\mathbf{V}_Q^{-H}\mathbf{G}^H\mathbf{G}\mathbf{V}_I^{-1}\mathbf{z}_I\right\}$$
$$+ j\mathbb{E}\left\{\mathbf{z}_I^H\mathbf{V}_I^{-H}\mathbf{G}^H\mathbf{G}\mathbf{V}_Q^{-1}\mathbf{z}_Q\right\}$$
$$+ \mathbb{E}\left\{\mathbf{z}_Q^H\mathbf{V}_Q^{-H}\mathbf{G}^H\mathbf{G}\mathbf{V}_Q^{-1}\mathbf{z}_Q\right\}.$$

If we assume that there is no remote channel distortion the equalization matrix $\mathbf{E}$ in (10) has all ones in its diagonal elements associated to the N_m used subcarriers, and zeros elsewhere. We also know from (40) that both Vandermonde matrices tend to be scaled unitary because the expected sampling instants are uniformly distributed and coincident for both branches. This also produces correlation between the elements of both noise samples vectors (14) and (16). Using these results we get

$$\sigma_e^2 = \frac{\sigma_z^2}{2N}\sum_{n=1}^{N_m}\left[\cos^2(\omega_c t_n) + \sin^2(\omega_c t_n)\right]$$
$$+ j\frac{\sigma_z^2}{2N}\sum_{n=1}^{N_m}\left[\frac{\sin(2\omega_c t_n)}{2} - \frac{\sin(2\omega_c t_n)}{2}\right]$$
$$= \frac{\sigma_z^2}{2N}N_m. \tag{41}$$

We can calculate the estimation error power per subcarrier as $\sigma_{e_n}^2 = \sigma_z^2/2N$. This error power is constant for a fixed noise power level and number of system subcarriers, independently of how many of them are actually transmitting a signal. We also see that the SICTAS receiver does not introduce an additional estimation error power, which means that it is able to improve the resulting signal-to-interference plus noise ratio (SINR) by totally eliminating the interference without incurring in a compromise situation which would be detrimental for its performance.

V. PERFORMANCE OF THE SICTAS RECEIVER

We evaluated the performance of our receiver by means of computer simulated transmissions of OFDM signals using system parameter combinations similar to the LTE-Advanced standard, as summarized in Table I. The guard bands were divided in two equal portions located at the bandwidth edges. Each

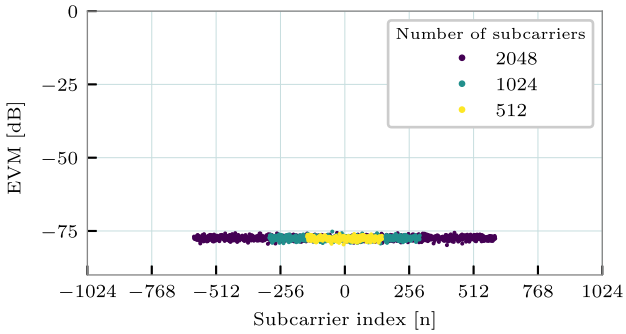

Fig. 4. Error vector magnitude per subcarrier for an 16-QAM OFDM system with the proposed receiver subject to −100 dB of SIR and 75 dB of SNR.

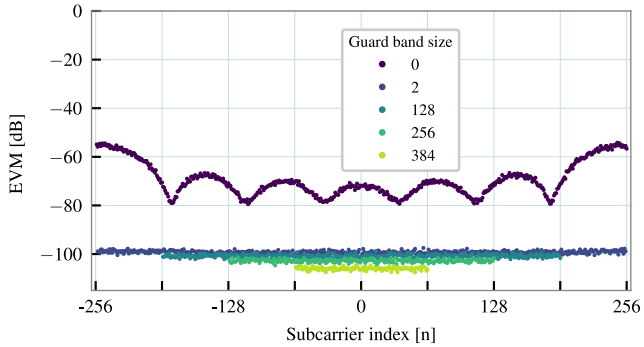

Fig. 5. Error vector magnitude per subcarrier for the SICTAS receiver demodulating a 16-QAM OFDM signal with different guard band sizes N_g, in a scenario with −100 dB of SIR and 100 dB of SNR.

transmission in our simulation consisted of a block with 7 OFDM symbols whose zero-frequency component does not transmit power, and the channels were considered constant during the individual symbol periods obtained from a subcarrier spacing of 15 kHz.

To verify if our method introduces any distortion depending on the subcarrier position we used following calculation for the error vector magnitude (EVM) at the n-th harmonic component

$$\mathrm{EVM}\,(n) = 20\log_{10}\sqrt{\frac{\mathbb{E}\left\{\left|\hat{w}_{n,r} - w_{n,r}\right|^2\right\}}{\mathbb{E}\left\{\left|w_{n,r}\right|^2\right\}}},$$

which measures the ratio between symbol error power and symbol power for each subcarrier, in decibels. The overall performance of the receiver was tested using the effective SINR

$$\mathrm{SINR} = 10\log_{10}\mathbb{E}\left\{\frac{\sigma_r^2}{\sigma_l^2 + \sigma_z^2}\right\},$$

with

$$\sigma_r^2 = \sum_{i=1}^{2N} \left|\tilde{x}_r\left(t_{I,i}\right)\right|^2 + \left|\tilde{x}_r\left(t_{Q,i}\right)\right|^2$$

$$\sigma_l^2 = \sum_{i=1}^{2N} \left|\tilde{x}_l\left(t_{I,i}\right) + s_{au}\left(t_{I,i}\right)\right|^2 + \left|\tilde{x}_l\left(t_{Q,i}\right) + s_{au}\left(t_{Q,i}\right)\right|^2$$

$$\sigma_z^2 = \sum_{i=1}^{2N} \left|z\left(t_{I,i}\right)\cos(\omega_c t_{I,i})\right|^2 + \left|z\left(t_{Q,i}\right)\sin(\omega_c t_{Q,i})\right|^2,$$

being respectively the signal power, the leaked interference-plus-auxiliary sampling signal power, and the noise power.

Fig. 4 shows the EVM in dB per subcarrier obtained for 10 independent realizations of the experiment, using settings exposed in Table I. The signal-to-noise ratio (SNR) was set to 75 dB, whereas the simulated signal-to-interference power ratio (SIR) was set to −100 dB in order to resemble an IBFD system without other SI suppression stages than the SICTAS receiver. For the same reason we also modeled the self-interference channel response with a Rician distribution corresponding to a loop-back link with a direct signal path. The remote channel was fixed with an ideal response.

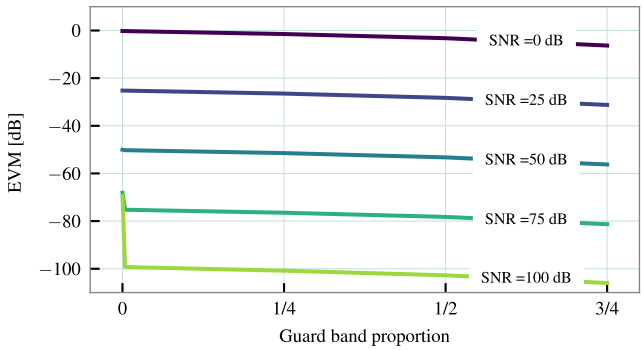

Fig. 6. Average error vector magnitude for an OFDM system using 512 subcarriers and varying guard band proportions, with SNR as a parameter.

We see from the results that, without dependence on the number of subcarriers used, the SICTAS receiver presents an uniform performance in the used bandwidth portion, without evidencing any distortions caused by our sampling and receive process. The EVM per subcarrier is exclusively limited by the noise power.

To test if the response is sensitive to the guard band proportion we simulated systems with a broad range of guard band sizes N_g. Fig. 5 shows the EVM in dB obtained per information-loaded subcarrier from a total of $2N = 512$ subcarriers, an interference power level producing a SIR of −100 dB, and a SNR of 100 dB.

The figure shows that if the higher frequency subcarriers transmit power the remaining ones suffer interference from them, as evidenced by the resultant EVM. This is deduced observing equations (20) and (22), which can be interpreted as two associated linear equation systems with the same unknown variables. If the extreme subcarriers are modulated with information there will be more unknowns than the $2N$ samples available to accurately demodulate the signal, and in these equations they introduce additional terms whose power is distributed over the whole signal bandwidth.

On the other hand, when the system employs guard bands the resulting EVM has always a flat response over the used spectrum with a value defined by the noise power level. This is further illustrated in Fig. 6, which shows the EVM averaged over all used subcarriers for the same system as previous simulation, but in this occasion with varying noise power at the receive port.

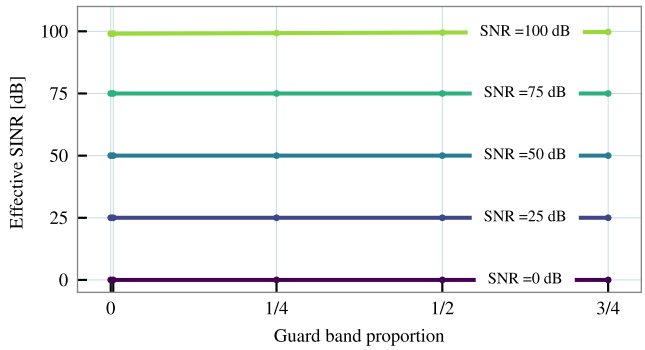

Fig. 7. Effective SINR for an OFDM system using 512 subcarriers and varying guard band proportions, with AWGN noise power as parameter and signal-to-interference ratio equal to −100 dB.

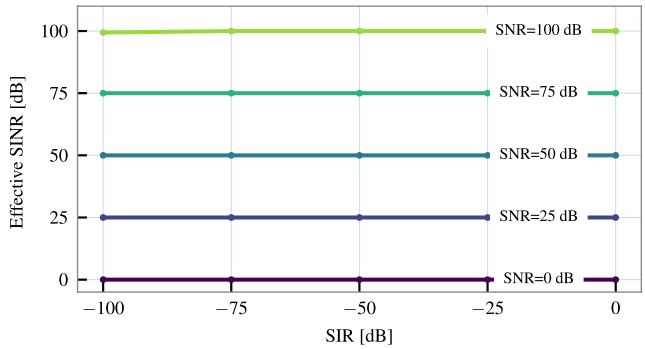

Fig. 8. Effective SINR obtained as a function of signal-to-interference power ratio for an OFDM system using a SICTAS receiver, with various SNR levels at the receive antenna.

The guard bands are also helpful to introduce oversampling in the SICTAS receiver because the polynomial order associated to the remote signal results smaller than the order of the polynomial for the self-interference plus auxiliary tone. This way, the desired signal cannot have as many zero-crossings as the SI and it is guaranteed that always a subset of the samples taken by the SICTAS receiver will have non-zero value.

We see that the different noise power levels impose limits on the system performance for the maximum number of usable subcarriers. Regarding the guard band proportions we can see that an increment of their size produces slight improvements on the results. This is in concordance with equation (41), since the estimation error power per subcarrier remains at the same level for increased guard band sizes, but the signal power is then divided by a decreasing number of used carriers N_m.

In Fig. 7 we show the effective SINR obtained after sampling a signal with different noise power levels and guard band proportions. We can observe in the results that our receiver eliminates the self-interference, and the samples carry only signal and noise power as the effective SINR equals the SNR.

Finally, the effects of different self-interference to signal power ratios for the same simulated system are presented in Fig. 8, where the effective SINR of the SICTAS sampled signal is shown again to be defined by the SNR. The performance of our receiver is the same for all self-interference power levels and does not depend on the presence of previous SI suppressors.

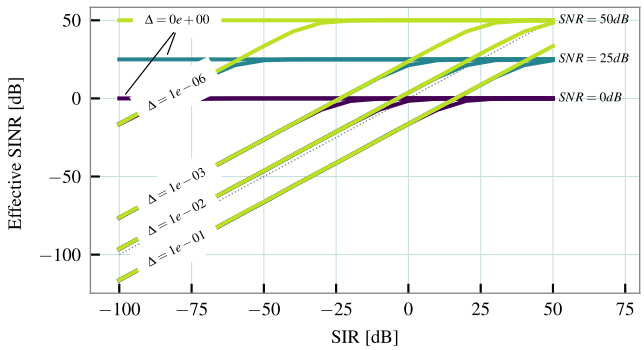

Fig. 9. Effective SINR as a function of SIR for a system with different sampling jitter ranges and SNR values.

A. *Effects of Sampling Time Error*

Sampling time error can be originated in different sources, e.g. loop-back channel estimation or in the zero-crossing calculations. When the signals that trigger the sample-and-hold are not perfectly coincident with the interference zero-crossings, a non-negligible portion of this high amplitude signal may leak into the samples taken by the SICTAS receiver. To illustrate the sensitivity to this imperfection in our system we added uniformly distributed error to the ideal self-interference zero-crossing instants, disregarding the source generating these time shifts. The samples obtained for both signal branches are taken at instants deviated from the ideal ones by a normalized quantity $\delta_{\{I,Q\},i}$ as follows

$$t_{\{I,Q\},i} = T\left(\tau_{\{I,Q\},i} + \delta_{\{I,Q\},i}\right), \tag{42}$$

where $0 \leq \tau_{\{I,Q\},i} < 1$ refers to the time variable normalized with respect to the OFDM symbol period T, as in (11) and (12). The errors are identically independently distributed variables $\delta_{\{I,Q\},i} \sim \mathcal{U}(-\Delta/2, \Delta/2)$, and Δ is the jitter range normalized with respect to the $2N$-th fraction of the symbol period T.

Fig. 9 shows the effective SINR obtained for a system with $2N = 512$ subcarriers, when only $N_m = 212$ from them are modulated with QPSK symbols. Simulations were run with varying signal-to-interference power ratios and with five different jitter ranges.

We see that when $\Delta = 0$ there is no sampling error, thus the ideal SICTAS receiver eliminates all the interference, and the effective SINR equals the SNR values used in our simulations. As the sampling jitter amplitude increases, more self-interference power leaks into the samples and the effective SINR is reduced with respect to the ideal case. For high SI power the performance is interference-limited, but we can see that for a jitter with range $\Delta = 10^{-3}$ the SICTAS receiver achieves 25 dB of SINR gain. When the jitter range increases beyond $\Delta = 10^{-2}$ the effective SINR results less than the SIR, evidencing that the performance degradation due to the SI is exacerbated by the sampling time error.

In Fig. 10 we expose more clearly the effects of applying different sampling jitter ranges to our model. It is evident by the curves that higher self-interference power levels demand more accurate timing in the sampling process in order to completely

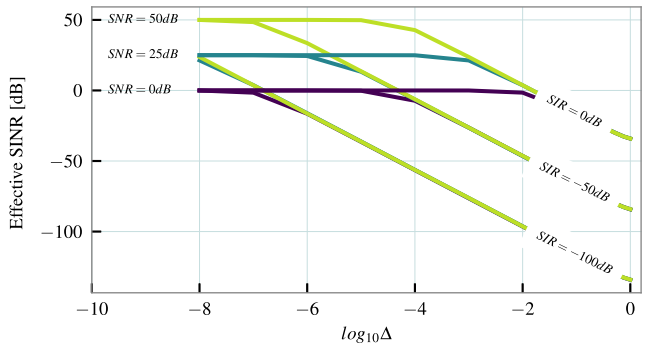

Fig. 10. Effect of sampling jitter range on the effective SINR for a SICTAS receiver with different SIR and SNR combinations.

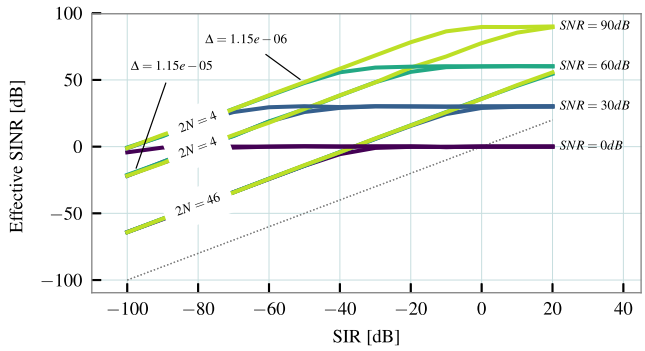

Fig. 11. Effective SINR for simulated systems replicating the setup of [26], with different numbers of subcarriers and jitter ranges Δ.

suppress interference and obtain a noise-limited system performance. Despite of that, we see that for $\Delta < 10^{-2}$ the effective SINR is greater than the SIR when our proposed receiver is used.

B. Performance Comparison With a Different SI Canceler

We present the comparison between our receiver affected by sampling time errors and the results in [26]. In this reference the authors prove that phase noise is the main performance limiter for their analog full-duplex cancelers. Besides, aligning the analog SI and cancelling signals in time domain and synchronizing zero-crossings for the SICTAS receiver may be seen as tasks of equivalent complexity achievable with similar hardware. This enables us to compare both techniques, although the fundamentals of the suppressors is different and may be subject to dissimilar limitations in practice.

We adapted our simulations to [26] using a system with $2N = 46$ subcarriers spaced 1 MHz from each other where only the one at index $n = 1$ transmits an unit amplitude symbol. The remaining subcarriers are muted, and the auxiliary sampling tones are located at $n = \pm 23$. Sampling jitter was considered uniform in distribution, and its standard deviation was set to $\sigma_\delta = 0.83$ ps to produce the same effects as the integrated circuit (IC) used in [26]. In our model this is equivalent to a jitter $\Delta = 1.32 \times 10^{-4}$.

The simulation results are shown in Fig. 11. We see that the SICTAS receiver achieves a maximal SI suppression of approximately 35 dB, which is the same result as in [26] when the authors use analog baseband cancellation. When the interference power decreases with respect to the signal, the performance is noise limited and the curves achieve the system SNR used in our simulations.

The average sampling rate in our system is twice the frequency of the auxiliary tones added before sampling the received signal. If we use less subcarriers to reduce this rate for a system with the same RMS phase noise, the jitter range Δ decreases because it is divided by a greater normalizing factor $T/2N$. This is clearly shown by the performance improvement in Fig. 11 when we set $2N = 4$ in our simulations, which corresponds to a single-carrier baseband system transmitting information in a 1 MHz carrier, and both auxiliary sampling signals placed at ± 2 MHz. When we maintain the sampling time error standard deviation at $\sigma_\delta = 0.83$ ps but reduce the average sampling rate to 4 MHz, the resulting jitter range is $\Delta = 1.15 \times 10^{-5}$. This effective jitter reduction causes the achieved SI suppression to equal 75 dB. When the clock signal source has less jitter, e.g. equivalent the one provided by the signal generator in the referenced article which produces $\Delta = 1.15 \times 10^{-6}$, the total performance is further increased providing an effective SINR which is approximately 100 dB.

From these results we see that with our method, even considering a major bottleneck like phase noise, it is possible to provide results comparable or superior to the digital canceler stages shown in Table I of [1].

VI. Conclusions

This article introduced a novel receiver structure to perform interference-free sampling of a desired signal in a full-duplex transmission. Our analysis evidences that by redistributing the sampling instants at the receiver it is possible to completely remove arbitrarily strong SI signals without relying on previous suppression stages, releasing the ADC dynamic range to accurately represent the signal of interest and enabling its further digital processing and demodulation.

Our results support the analysis presented for a simplified scenario, yet there are numerous aspects regarding a practical implementation of this technique which have to be addressed in future developments. However, with this work we proved that the SICTAS receiver is the essence of a promising solution towards fully-digital self-interference cancellation in IBFD applications, which may extend its benefits to smaller, cheaper and energy-efficient communication devices.

Appendix
Unimodular Roots of Polynomials Associated to Baseband OFDM Signals

Let us define a polynomial $P(z)$ as in (27) using the coefficients defined either in (36) or in (37), which correspond to the real and imaginary parts of baseband OFDM signal added to a cosine with the highest subcarrier frequency. The polynomial will have all its roots on the unit circle, with multiplicity one, if any of the conditions (28) to (30) is satisfied [23].

A. Verification of Condition (28)

By the definition of coefficients $\tilde{a}_{n,l}$ in (34), and using them in (28) we obtain

$$\begin{aligned}|\tilde{a}_{N,l}| &> \frac{1}{2}\sum_{n=-N}^{N-1}|\tilde{a}_{n+1,l}-\tilde{a}_{n,l}|\\ A_{au} &> \frac{1}{2}\Big(\big|\tilde{w}_{-N+1,l}+\tilde{w}^*_{N-1,l}-A_{au}\big|\\ &\quad+\sum_{n=-N+1}^{N-2}\big|\tilde{w}_{n+1,l}+\tilde{w}^*_{-n-1,l}-\tilde{w}_{n,l}-\tilde{w}^*_{-n,l}\big|\\ &\quad+\big|A_{au}-\tilde{w}_{N-1,l}-\tilde{w}^*_{-N+1,l}\big|\Big),\end{aligned}$$

whereas using coefficients $\tilde{b}_{n,l}$ defined by (35) in the same condition produces

$$\begin{aligned}\left|\tilde{b}_{N,l}\right| &> \frac{1}{2}\sum_{n=-N}^{N-1}\left|\tilde{b}_{n+1,l}-\tilde{b}_{n,l}\right|\\ A_{au} &> \frac{1}{2}\Big(\big|\tilde{w}^*_{N-1,l}-\tilde{w}_{-N+1,l}-A_{au}\big|\\ &\quad+\sum_{n=-N+1}^{N-2}\big|\tilde{w}^*_{-n-1,l}-\tilde{w}_{n+1,l}-\tilde{w}^*_{-n,l}+\tilde{w}_{n,l}\big|\\ &\quad+\big|A_{au}-\tilde{w}^*_{-N+1,l}+\tilde{w}_{N-1,l}\big|\Big).\end{aligned}$$

By the triangle inequality we can unify both results as

$$\begin{aligned}A_{au} &> A_{au}+|\tilde{w}_{N-1,l}|+|\tilde{w}_{-N+1,l}|\\ &\quad+\frac{1}{2}\sum_{n=-N+1}^{N-2}|\tilde{w}_{-n-1,l}|+|\tilde{w}_{n+1,l}|+|\tilde{w}_{-n,l}|+|\tilde{w}_{n,l}|.\end{aligned}$$

We defined in Section IV that $A_{au}>0$, and since all terms in the right member of the last expression are greater than zero, condition (28) can not be satisfied for real OFDM signals with an added cosine.

B. Verification of Condition (29)

Replacing for $\tilde{a}_{n,l}$ in (29) results

$$\begin{aligned}|\tilde{a}_{N,l}| &> \sum_{n=-N+1}^{N-1}|\tilde{a}_{N,l}-\tilde{a}_{n,l}|\\ A_{au} &> \sum_{n=-N+1}^{N-1}\left|A_{au}-\tilde{w}_{n,l}-\tilde{w}^*_{-n,l}\right|,\end{aligned}$$

and the same condition for the coefficients $\tilde{b}_{n,l}$ results in

$$\begin{aligned}\left|\tilde{b}_{N,l}\right| &> \sum_{n=-N+1}^{N-1}\left|\tilde{b}_{N,l}-\tilde{b}_{n,l}\right|\\ A_{au} &> \sum_{n=-N+1}^{N-1}\left|A_{au}-\tilde{w}^*_{-n,l}+\tilde{w}_{n,l}\right|.\end{aligned}$$

By the triangle inequality we unify these results as

$$A_{au} > (2N-1)\,A_{au}+\sum_{n=-N+1}^{N-1}|\tilde{w}_{n,l}|+\left|\tilde{w}^*_{-n,l}\right|.$$

Again, since $A_{au}>0$ this result can never be satisfied, and therefore condition (29) cannot be achieved by a real OFDM signal added to a cosine signal.

C. Verification of Condition (30)

Using the definition of coefficients $\tilde{a}_{n,l}$ in (30) results in

$$\begin{aligned}|\tilde{a}_{N,l}| &> \frac{1}{2}\sum_{n=-N+1}^{N-1}|\tilde{a}_{n,l}|\\ A_{au} &> \frac{1}{2}\sum_{n=-N+1}^{N-1}\left|\tilde{w}_{n,l}+\tilde{w}^*_{-n,l}\right|\\ &> |\Re\{\tilde{w}_{0,l}\}|+\sum_{n=1}^{N-1}\left|\tilde{w}_{n,l}+\tilde{w}^*_{-n,l}\right|.\end{aligned}\tag{43}$$

Inserting the coefficients $\tilde{b}_{n,l}$ in the same condition produces

$$\begin{aligned}\left|\tilde{b}_{N,l}\right| &> \frac{1}{2}\sum_{n=-N+1}^{N-1}\left|\tilde{b}_{n,l}\right|\\ A_{au} &> \frac{1}{2}\sum_{n=-N+1}^{N-1}\left|\tilde{w}^*_{-n,l}-\tilde{w}_{n,l}\right|\\ &> |\Im\{\tilde{w}_{0,l}\}|+\sum_{n=1}^{N-1}\left|\tilde{w}_{n,l}-\tilde{w}^*_{-n,l}\right|.\end{aligned}\tag{44}$$

Both results (43) and (44) are unified by

$$\begin{aligned}A_{au} &> \max\left(|\Re\{\tilde{w}_{0,l}\}|,|\Im\{\tilde{w}_{0,l}\}|\right)\\ &\quad+\sum_{n=1}^{N-1}\max\left(\left|\tilde{w}_{n,l}+\tilde{w}^*_{-n,l}\right|,\left|\tilde{w}_{n,l}-\tilde{w}^*_{-n,l}\right|\right),\end{aligned}$$

and if we use the triangle inequality in addition to

$$\max\left(|\Re\{\tilde{w}_{0,l}\}|,|\Im\{\tilde{w}_{0,l}\}|\right)\le|\tilde{w}_{0,l}|,$$

the condition on A_{au} results

$$A_{au} > \sum_{n=-N+1}^{N-1}|\tilde{w}_{n,l}|.\tag{45}$$

This means that the amplitude of the cosine signal has to be greater than the sum of amplitudes of all symbols modulating the remaining OFDM subcarriers.

REFERENCES

[1] D. Kim, H. Lee, and D. Hong, "A survey of in-band full-duplex transmission: From the perspective of PHY and MAC layers," *IEEE Commun. Surveys Tut.*, vol. 17, no. 4, pp. 2017–2046, Feb. 2015.

[2] S. Hong *et al.*, "Applications of self-interference cancellation in 5g and beyond," *IEEE Commun. Mag.*, vol. 52, no. 2, pp. 114–121, Feb. 2014. [Online]. Available: http://ieeexplore.ieee.org/stamp/stamp.jsp?arnumber=6736751

[3] I. Krikidis and G. Zheng, *Advanced Relay Technologies in Next Generation Wireless Communications*. Stevenage, U.K.: Inst. Eng. Technol., 2016.

[4] A. Sabharwal, P. Schniter, D. Guo, D. W. Bliss, S. Rangarajan, and R. Wichman, "In-band full-duplex wireless: Challenges and opportunities," *IEEE J. Sel. Areas Commun.*, vol. 32, no. 9, pp. 1637–1652, Sep. 2014.

[5] M. Jain *et al.*, "Practical, real-time, full duplex wireless," in *Proc. 17th Annu. Int. Conf. Mobile Comput. Netw.*, 2011, pp. 301–312. [Online]. Available: http://dl.acm.org/citation.cfm?id=2030647

[6] J. Zhou and H. Krishnaswamy, "Recent developments in fully-integrated RF self-interference cancellation for frequency-division and full-duplex radios," in *Proc. IEEE 81st Veh. Technol. Conf.*, May 2015, pp. 1–5.

[7] J. I. Choi, S. Hong, M. Jain, S. Katti, P. Levis, and J. Mehlman, "Beyond full duplex wireless," in *Proc. Conf. Rec. 46th Asilomar Conf. Signals Syst. Comput.*, Nov. 2012, pp. 40–44.

[8] D. Korpi, T. Riihonen, V. Syrjälä, L. Anttila, M. Valkama, and R. Wichman, "Full-duplex transceiver system calculations: Analysis of ADC and linearity challenges," *IEEE Trans. Wireless Commun.*, vol. 13, no. 7, pp. 3821–3836, Jul. 2014.

[9] C. A. Schmidt, G. González, F. Gregorio, J. E. Cousseau, T. Riihonen, and R. Wichman, "Compensation of adc-induced distortion in broadband full-duplex transceivers," in *Proc. IEEE Int. Conf. Commun. Workshops*, 2017, pp. 1147–1152. [Online]. Available: http://ieeexplore.ieee.org/document/7962813/

[10] F. Eng, "Non-uniform sampling in statistical signal processing," Ph.D. dissertation, Institutionen för Systemteknik, Linköping, Sweden, 2007.

[11] A. J. Jerri, "The Shannon sampling theorem —its various extensions and applications: A tutorial review," *Proc. IEEE*, vol. 65, no. 11, pp. 1565–1596, Nov. 1977.

[12] F. Marvasti, M. Analoui, and M. Gamshadzahi, "Recovery of signals from nonuniform samples using iterative methods," *IEEE Trans. Signal Process.*, vol. 39, no. 4, pp. 872–878, Apr. 1991.

[13] F. Marvasti, Ed., *Nonuniform Sampling: Theory and Practice*. New York, NY, USA: Springer, 2001.

[14] Y.-P. Lin and P. P. Vaidyanathan, "Periodically nonuniform sampling of bandpass signals," *IEEE Trans. Circuits Syst. II, Analog Digit. Signal Process.*, vol. 45, no. 3, pp. 340–351, Mar. 1998.

[15] F. Marvasti, "Nonuniform sampling theorems for bandpass signals at or below the Nyquist density," *IEEE Trans. Signal Process.*, vol. 44, no. 3, pp. 572–576, Mar. 1996.

[16] N. K. Sharma and T. V. Sreenivas, "Event-triggered sampling using signal extrema for instantaneous amplitude and instantaneous frequency estimation," *Signal Process.*, vol. 116, pp. 43–54, 2015.

[17] H. Ishibashi, H. Suzuki, K. Fukawa, and S. Suyama, "Application of real zero concept to coherent detector for quadrature amplitude modulation," in *Proc. 21st Annu. IEEE Int. Symp. Pers. Indoor Mobile Radio Commun.*, Sep. 2010, pp. 597–602.

[18] P. Diniz, W. Martins, and M. Lima, *Block Transceivers: OFDM and Beyond* (Synthesis Lectures on Communications). San Rafael, CA, USA: Morgan Claypool Publ., 2012.

[19] F. Soto-Eguibar and H. Moya-Cessa, "Inverse of the vandermonde and vandermonde confluent matrices," *Appl. Math. Inf. Sci.*, vol. 5, pp. 361–366, 2011.

[20] L. R. Turner, "Inverse of the vandermonde matrix with applications," *NASA Techn. Note D-3547*, Aug. 1966. [Online]. Available: https://ntrs.nasa.gov/archive/nasa/casi.ntrs.nasa.gov/19660023042.pdf

[21] M. E. El-Mikkawy, "Explicit inverse of a generalized vandermonde matrix," *Appl. Math. Comput.*, vol. 146, no. 2, pp. 643–651, 2003.

[22] H. B. Voelcker, "Toward a unified theory of modulation part i: Phase-envelope relationships," *Proc. IEEE*, vol. 54, no. 3, pp. 340–353, Mar. 1966.

[23] Y. Choo and Y.-J. Kim, "On the zeros of self-inversive polynomials," *Int. J. Math. Anal.*, vol. 7, pp. 187–193, 2013.

[24] S. Kay and R. Sudhaker, "A zero crossing-based spectrum analyzer," *IEEE Trans. Acoustics, Speech, Signal Process.*, vol. 34, no. 1, pp. 96–104, Feb. 1986.

[25] G. A. Sitton, C. S. Burrus, J. W. Fox, and S. Treitel, "Factoring very-high-degree polynomials," *IEEE Signal Process. Mag.*, vol. 20, no. 6, pp. 27–42, Nov. 2003.

[26] A. Sahai, G. Patel, C. Dick, and A. Sabharwal, "On the impact of phase noise on active cancellation in wireless full-duplex," *IEEE Trans. Veh. Technol.*, vol. 62, no. 9, pp. 4494–4510, Nov. 2013. [Online]. Available: http://ieeexplore.ieee.org/stamp/stamp.jsp?arnumber=6523998

Micael Bernhardt received the B.Sc. degree in electronic engineering from the Universidad Nacional de Misiones, Oberá, Argentina, in 2011. He is currently working toward the Ph.D. degree at the Signal Processing and Communication Laboratory, Universidad Nacional del Sur, Bahía Blanca, Argentina.

His research interests include digital communications, digital signal processing algorithms, and resource-efficient wireless communications and networks.

Fernando Gregorio received the B.Sc. degree from the Universidad Tecnologica Nacional, Bahía Blanca, Argentina, the M.Sc. degree in electrical engineering from the Universidad Nacional del Sur (UNS), Bahía Blanca, and the D.Sc. degree in electrical engineering from the Helsinki University of Technology, Espoo, Finland, in 2007.

Since 2008, he has been with the Departmento de Ingeniería Eléctrica y de Computadoras, UNS. He is currently a Senior Researcher with the Consejo Nacional de Investigaciones Científicas y Técnicas, Argentina. His research interests include power amplifier nonlinearities and RF imperfection in MIMO-OFDM systems and multiuser communications.

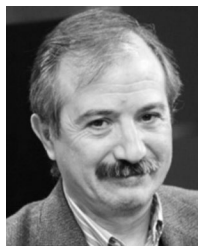

Juan Cousseau (S'84–M'94–SM'00) was born in Mar del Plata, Argentina. He received the B.Sc. degree from the Universidad Nacional del Sur (UNS), Bahia Blanca, Argentina, in 1983, and the M.Sc. and Ph.D. degrees from COPPE/Universidade Federal do Rio de Janeiro, Rio de Janeiro, Brazil, in 1989, and 1993, respectively, all in electrical engineering.

Since 1984, he has been with the undergraduate Department of Electrical and Computer Engineering, UNS. He has also been with the graduate Program at the same university since 1994. He is a Senior Researcher of the National Scientific and Technical Research Council of Argentina. He has been involved in scientific and industry projects with research groups from Argentina, Brazil, Spain, USA, Finland, and South Africa. He is a coordinator of the Signal Processing and Communication Laboratory at UNS (http://lapsyc.ingelec.uns.edu.ar). His research interests include adaptive and statistical signal processing with application to modern broadband wireless communications. He was the IEEE Circuits and Systems Chair of the Argentine Chapter, from 1997 to 2000, and member of the Executive Committee of the IEEE Circuits and Systems Society during 2000–2001 (Vice-president for Region 9). He participates of the IEEE Signal Processing Society Distinguished Lecturer Program 2006. He was Chair of the Municipal Agency of Science and Technology of Bahía Blanca city, Argentina. He is the Director of the "Instituto de Investigaciones en Ingeniería Eléctrica—Alfredo Desages," CONICET—UNS (http://www.iiie.uns.edu.ar).

Taneli Riihonen (S'06–M'14) received the D.Sc. degree in electrical engineering (with distinction) from Aalto University, Espoo, Finland, in August 2014. He is currently an Assistant Professor with the Laboratory of Electronics and Communications Engineering, Tampere University of Technology, Tampere, Finland. He held various research positions with the Helsinki University of Technology and Aalto University School of Electrical Engineering from September 2005 to December 2017. He was a Visiting Associate Research Scientist and an Adjunct Assistant Professor with Columbia University, New York, NY, USA, from November 2014 to December 2015. His research interests include physical-layer OFDM(A), multiantenna, relaying, and full-duplex wireless techniques with current interest in the evolution of beyond 5G systems. He has been nominated eleven times as an Exemplary/Top Reviewer of various IEEE journals and is serving as an Editor for the IEEE COMMUNICATIONS LETTERS since October 2014 and for the IEEE WIRELESS COMMUNICATIONS LETTERS since May 2017. He was the recipient of the Finnish technical sector's award for the best doctoral dissertation of the year and the EURASIP Best Ph.D. Thesis Award 2017.